# Structural Examination of the Nickel Site in *Chromatium vinosum* Hydrogenase: Redox State Oscillations and Structural Changes Accompanying Reductive Activation and CO Binding†

Gerard Davidson,‡ Suranjan B. Choudhury,‡ Zhijie Gu,‡ Kurethara Bose,‡ Winfried Roseboom,§ Simon P. J. Albracht,§ and Michael J. Maroney*,‡

*Department of Chemistry, University of Massachusetts, Amherst, Massachusetts 01003 and the E. C. Slater Institute, Biochemistry, University of Amsterdam, Plantage Muidergracht 12 NL-1018 TV Amsterdam, The Netherlands*

*Received February 8, 2000; Revised Manuscript Received April 12, 2000*

ABSTRACT: An X-ray absorption spectroscopic study of structural changes occurring at the Ni site of *Chromatium vinosum* hydrogenase during reductive activation, CO binding, and photolysis is presented. Structural details of the Ni sites for the ready silent intermediate state, $SI_r$, and the carbon monoxide complex, SI−CO, are presented for the first time in any hydrogenase. Analysis of nickel K-edge energy shifts in redox-related samples reveals that reductive activation is accompanied by an oscillation in the electron density of the Ni site involving formally Ni(III) and Ni(II), where all the EPR-active states (forms A, B, and C) are formally Ni(III), and the EPR-silent states are formally Ni(II). Analysis of XANES shows that the Ni site undergoes changes in the coordination number and geometry that are consistent with five-coordinate Ni sites in forms A, B, and $SI_u$; distorted four-coordinate sites in $SI_r$ and R; and a six-coordinate Ni site in form C. EXAFS analysis reveals that the loss of a short Ni−O bond accounts for the change in coordination number from five to four that accompanies formation of $SI_r$. A shortening of the Ni−Fe distance from 2.85(5) Å in form B to 2.60(5) Å also occurs at the SI level and is thus associated with the loss of the bridging O-donor ligand in the active site. Multiple-scattering analysis of the EXAFS data for the SI−CO complex reveals the presence of Ni−CO ligation, where the CO is bound in a linear fashion appropriate for a terminal ligand. The putative role of form C in binding $H_2$ or $H^-$ was examined by comparing the XAS data from form C with that of its photoproduct, form L. The data rule out the suggestion that the increase in charge density on the NiFe active site that accompanies the photoprocess results in a two-electron reduction of the Ni site [Ni(III) → Ni(I)] [Happe, R. P., Roseboom, W., and Albracht, S. P. J. (1999) *Eur. J. Biochem. 259*, 602−608]; only subtle structural differences between the Ni sites were observed.

Hydrogenases ($H_2$ases) are enzymes that catalyze the two-electron redox chemistry of hydrogen gas. As such, they are important enzymes in the metabolism of many microorganisms (*1*). Hydrogenases can be used to oxidize $H_2$ to produce reducing equivalents or to generate $H_2$ during fermentation, where protons serve as the terminal electron acceptor in an electron transport chain. The use of this chemistry in a vectorial fashion across membranes may be a primitive mechanism for generating proton gradients (*2*). The known $H_2$ases can be divided into groups based on the inorganic cofactors that are present. The largest group of $H_2$ases contain Ni, Fe, and $S^{2-}$ as inorganic constituents ([NiFe]-$H_2$ases) (*3*). In addition, a small group of enzymes that contain only Fe and $S^{2-}$ have been identified ([Fe]-$H_2$ases) (*4*). An enzyme that contains no known inorganic cofactors and is involved in the reduction of methylenetetrahydromethanopterin has been isolated from *Methanobacterium* species (*5*).

The $H_2$ase isolated from *Chromatium vinosum*, a purple-sulfur, photosynthetic bacterium, is a typical member of the [NiFe] group in that it is composed of two subunits of about 34 and 60 kDa and contains approximately one Ni and 12 Fe atoms per holoenzyme (*6*). Most of the Fe is distributed among three Fe−S clusters; two $Fe_4S_4$ and one $Fe_3S_4$ clusters have been detected by Mössbauer and EPR studies (*3*, *7*). Like most of the [NiFe]-$H_2$ases, the enzyme from *C. vinosum* exhibits a number of redox-dependent EPR signals at 77 K that exhibit $^{61}$Ni hyperfine splittings when the enzyme is isotopically enriched (*3*, *8*). These signals include those associated with as-isolated oxidized and catalytically inactive enzymes [form A (unready): $g = 2.31, 2.23, 2.02$; form B (ready): $g = 2.34, 2.16, 2.01$] and a two-electron reduced active form of the enzyme (form C: $g = 2.19, 2.16, 2.02$) (*6*).

† This research was supported by grants from the National Institutes of Health (GM38829, M.J.M.), The Netherlands Organization for Scientific Research (NWO), and The Netherlands Foundation for Chemical Research (SON). Data were collected at the National Synchrotron Light Source (NSLS) Brookhaven National Laboratory, which is supported by the U.S. Department of Energy, Division of Materials Sciences and Division of Chemical Sciences. Beamline X9B at NSLS is supported in part by NIH Grant RR-01633.

* To whom correspondence should be addressed at Department of Chemistry, Lederle Graduate Research Center Tower A, University of Massachusetts, Amherst, MA 01003-4510. Phone: 413-545-4876. FAX: 413-545-4490. E-mail: Mmaroney@chem.umass.edu.

‡ University of Massachusetts.

§ University of Amsterdam.

10.1021/bi000300t CCC: $19.00 
Published on Web 06/02/2000

Scheme 1

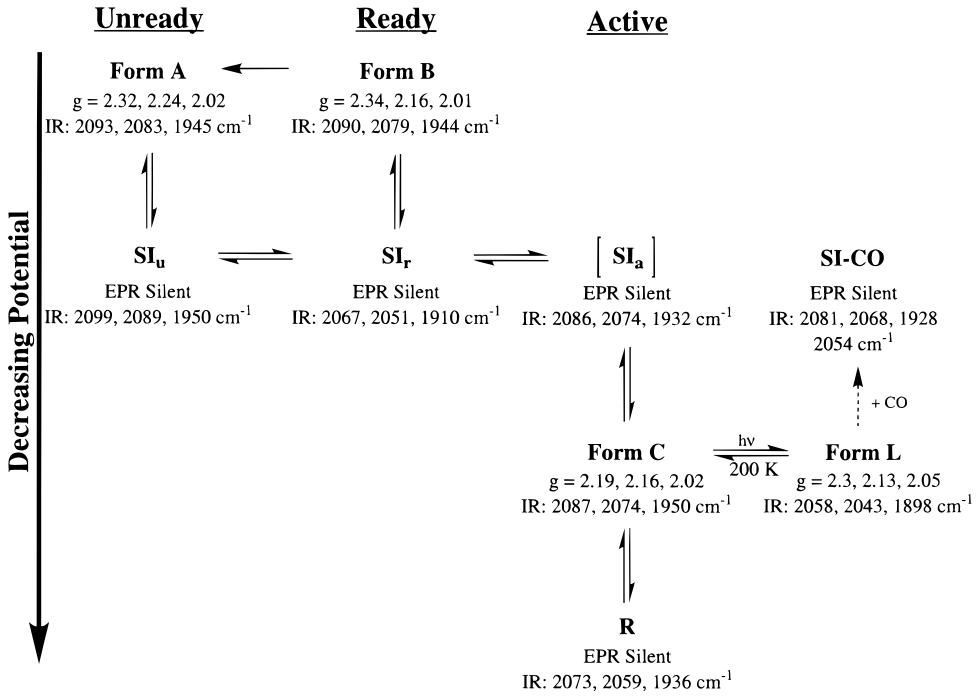


Reductive activation (Scheme 1) of the enzyme by $H_2$ or low-potential reductants at 30° results in the loss of the EPR signals associated with forms A and B and the appearance of the EPR signal of form C (*9*, *10*). This reduction occurs readily for form B but has a long lag phase (hours) for form A. Thus, form B represents a "ready" state of the enzyme, and form A is an "unready" state. In redox titrations performed at 30°, forms A and B are in redox equilibrium with the EPR-silent (SI) one-electron reduction products. However, if the titration is performed at 2°, the reductions of both forms A and B proceed to form spectroscopically distinct EPR-silent forms (*11*), $SI_u$ and $SI_r$, respectively, that do not interconvert at low temperature. Form B is irreversibly reduced at 2° (*12*). Both the $SI_u$ and the $SI_r$ states represent catalytically inactive states of the enzyme.

The $SI_u$ state cannot be further reduced at 2°, whereas $SI_r$ is reduced very slowly to form C (*12*). A third form of the one-electron reduced and EPR-silent state, $SI_a$, has been shown to be involved in producing form C (*12*). This catalytically active EPR-silent intermediate is in slow equilibrium with $SI_r$ (*12*). One-electron reduction of $SI_a$ gives rise to form C, the EPR-active reduced state of the enzyme. Under a $H_2$ atmosphere, form C is further reduced to R, the fully reduced state of the enzyme. Form C is photochemically labile and can be converted to an EPR-active state, form L ($g$ = 2.3, 2.13, 2.05), by exposure to light at 77 K (*13*). Form C is regained by annealing the sample in the dark at ca. 200 K. The conversion of form C to form L has been probed using ENDOR spectroscopy (*14*), which revealed a solvent-exchangeable proton(s) coupled to the electron spin at the active site in form C that is lost upon conversion to form L. The site of attachment of this proton in the active site has not yet been established. Recent pre-steady-state kinetic measurements have revealed that CO, an inhibitor of $H_2$ase, binds to form C to produce a thermally stable product that is EPR-silent, SI−CO (*15*). The binding site for CO in this EPR-silent state has not been established, but kinetic and EPR data on the photolytically produced transient adduct with form L, form L−CO, indicate that the CO binds to Ni, possibly in a bridging mode with the active site Fe atom. The relationship between the eight states of the enzyme discussed above is summarized in Scheme 1.

Knowledge of the structure of the active site of [NiFe]-$H_2$ases was greatly enhanced by the 2.85-Å resolution crystal structure of the [NiFe]-$H_2$ase from *Desulfovibrio gigas* (*16*) and then again by the 2.54-Å resolution structure (*17*, *18*). The similarity between the respective EPR (*3*, *19*), IR (*11*, *17*, *20*−*22*), Mössbauer (*7*, *23*), and XAS spectra (*24*) obtained from the *D. gigas* and *C. vinosum* $H_2$ases, in addition to identical cofactor composition in the two enzymes, indicates that the structures of these enzymes are likely to be very similar. The crystal structures of *D. gigas* $H_2$ase provided information about the spatial arrangement of the cofactors, revealing that the Ni site is part of a heterodinuclear active site involving an Fe center bridged to the Ni by a pair of cysteine thiolates (Cys 68 and Cys 533) and a third low Z atom, X (*17*). As a consequence of the short Ni−X distance found (1.7 Å), it was postulated that X represents a Ni-oxo group that bridges to the Fe (Fe−X = 2.1 Å). The remaining ligands involved in the Ni site are two terminally bound cysteine thiolates (Cys 65 and Cys 530). Analysis of the Ni−S distances in the active site indicated that the terminal ligands have significantly shorter bonds (2.3 and 2.2 Å) than the bonds formed by the bridging cysteines (2.6 Å). Analysis of the EPR spectrum of the crystals used in the crystallographic study shows that the crystal was ∼40% form A, ∼10% form B, and 50% EPR-silent (probably mostly $SI_u$).

The crystal structure also revealed that the Fe site has a unique structure (*16*, *17*). In addition to the cysteinate bridging ligands, the Fe was shown to be coordinated by three nonprotein ligands. Analysis of IR spectra obtained from samples of the *C. vinosum* enzyme was used to assign these ligands to a pair of $CN^-$ ligands and a CO ligand (*25*,

*26*). These assignments are in complete agreement with data obtained from a model compound, ($\eta^5$-$C_5H_5$)Fe(CN)$_2$CO (*27*). The electron density associated with the nonprotein ligands in the structure is also consistent with these diatomic molecules (*17*). Further, the stretching frequencies vary with redox poise in the same manner as the EPR signals (Scheme 1), providing a spectral probe of the EPR-silent states (*11*, *20*). The Fe site has been found to be a low-spin Fe(II) center in the EPR-active forms by both $^{57}$Fe ENDOR (*28*) and EPR studies (*29*), consistent with earlier studies of the *C. vinosum* enzyme using Mössbauer spectroscopy (*7*).

X-ray absorption spectroscopy (XAS) has been used to provide electronic and molecular structural information regarding the Ni site complementary to the information obtained by crystallographic studies and from other spectroscopic techniques (*14*, *24*, *30*−*35*). Since the analysis of extended X-ray absorption fine structure (EXAFS) provides metric details of the Ni site at a higher precision than is available from the crystal structure (typically ±0.02 Å for distances in the primary coordination sphere) and does not require crystalline samples, it is particularly useful in studying the details of the Ni site structure and the effects of redox poise on the structure of the Ni site. We report here a study of the structure of the Ni site in *C. vinosum* $H_2$ase involving samples poised in the eight distinct states (forms A and B, $SI_u$, $SI_r$, SI−CO, forms C and L, and R) in view of recent crystallographic studies of *D. gigas* and *Desulfomicrobium baculatum* $H_2$ases. The XAS studies presented were specifically designed to examine the presence/absence of a Ni−O ligand as a function of redox poise, to test the binding of CO to the Ni site and provide metric details of the complex formed, and to examine variations in the Ni−Fe distance as a function of redox poise. Of the samples examined, the $SI_r$ state and the SI−CO adduct are structurally examined for the first time in any $H_2$ase. The inclusion of $SI_r$ further clarifies the redox role of the Ni site.

## EXPERIMENTAL PROCEDURES

*Enzyme and XAS Sample Preparation.* The sample preparation and XAS data for samples of *C. vinosum* $H_2$ase poised in form A, form B, $SI_u$, form C, and form R have been previously reported (*24*). Data obtained from new samples of form C were used in the analysis of the data from this form. Samples poised in the $SI_r$, SI−CO, and form L states are reported for the first time and were prepared as follows.

*(1) $SI_r$.* Enzyme was converted to form B (90% by EPR) as described previously (*24*). To a concentrated enzyme solution (1.5 mM in 50 mM MES buffer, pH 6.0, cooled in ice) was added: (i) 50 μM of the mediators 2,3,5,6-tetramethyl-*p*-phenylenediamine ($E'_o$ = +275 mV), 2,6-dichlorophenolindophenol ($E'_o$ = +230 mV), 1,2-naphthoquinone-4-sulfonic acid ($E'_o$ = +215 mV), phenazine methosulfate ($E'_o$ = +80 mV), and methylene blue ($E'_o$ = +11 mV); (ii) submitochondrial particles (0.4 mg) (*36*), 80 mM succinate, and 8 μM cytochrome *c* (horse heart). It was then loaded in the XAS cuvette, put under 10% $H_2$, 90% Ar, kept in ice for 30 min, and then frozen in liquid nitrogen. The sample (final enzyme concentration 1.2 mM) showed a small EPR signal from form C (53 μM or 4.5% of the enzyme concentration). Addition of the mediators, submitochondrial particles, cytochrome *c*, and succinate ensured optimal removal of $O_2$ (via the cytochrome *c* oxidase in the particles). Some $H_2$ (10%) was added to further decrease the potential (via reaction with the enzyme) for the complete reduction of form B to $SI_r$. The low temperature prevented activation of the $H_2$ase (*12*), as was verified by parallel experiments with dilute enzyme, in which the $H_2$-uptake activity with benzyl viologen and methylene blue was measured. Given the purity of the form B sample (90%) and the EPR spectrum of the reduced XAS sample (4.5% form C, the rest EPR-silent), the sample was 85% poised in the inactive $SI_r$ state.

*(2) SI−CO.* The enzyme was fully reduced and activated by incubation under $H_2$ for 30 min at 50°. After cooling, the $H_2$ gas was replaced by CO. The FTIR spectrum of samples similarly prepared is homogeneous, and the published IR spectrum shows a peak assigned to bound extrinsic CO ($\nu_{CO}$ = 2054 cm$^{-1}$) (*21*).

*(3) Form L.* Exposure of form C to visible light leads to the formation of form L, which is stable below 100 K. A single sample of form C frozen into two XAS sample holders was used to collect the data for the form C/form L comparison. One of these samples was used to prepare the form L sample by irradiating it in liquid $N_2$, as previously described for *Thiocapsa roseopersicina* $H_2$ase samples (*14*). The sample was monitored by EPR and irradiated until conversion of form C to form L was achieved. The sample was handled cold, and its integrity following data collection was confirmed by EPR spectroscopy.

*XAS Data Collection and Analysis.* XAS data for all samples was taken on beam line X9 at the National Synchroton Radiation Laboratory (NSLS) at Brookhaven National Laboratory during several runs. The samples were contained in polycarbonate holders that allowed collection of the XAS and EPR data without thawing the samples. These holders were inserted into slotted aluminum holders that were held near 50 K by using a He displex cryostat for XAS data collection. Data were collected as previously described (*32*), under dedicated conditions at 2.58 GeV and 120−200 mA. For edge studies, a Si(220) double crystal monochromator internally calibrated to the first inflection point of Ni foil (8331.6 eV) was used. This arrangement provides a theoretical resolution of ca. 0.5 eV for the 0.5-mm hutch slit height employed. The spectra obtained using 0.2-eV steps had edge energies that were reproducible to within ±0.1 eV. This value is used as an estimated error for the edge energy measurements in Table 1, except for form C.

For EXAFS data collection, in which energy resolution is less important, some of the data were collected using a Si(111) double crystal monochromator with a 1-mm hutch slit height, for the additional X-ray intensity that this arrangement provided. Harmonic rejection was accomplished with a focusing mirror left flat. X-ray fluorescence data were collected using a 13-element Ge detector (Canberra). A 4-μs dead time correction was employed in analyzing the data from this detector with internal count rate <40 000 Hz.

The integrity of the samples after ~12 h of exposure to monochromatic synchrotron radiation was monitored in three ways. First, EPR spectra taken before and after exposure were compared. Second, the energy of the Ni K-edge obtained from each sample was monitored on sequential scans. Third, some of the samples were assayed for either $H_2$-evolution

Table 1: Ni K-edge and XANES Data for *Chromatium vinosum* Hydrogenase

| sample | Ni K-edge energy (eV) | $E - E_{ave}$ (eV)[a] | 1s → 3d peak area ($10^{-2}$ eV) | ref |
|---|---|---|---|---|
| form A | 8340.0(1) | +0.6 | 7.6(5) | *24* |
| form B | 8340.4(1) | +1.0 | 6.3(5) | *24* |
| $SI_u$ | 8339.8(1) | +0.4 | 5.6(5) | this work |
| $SI_r$ | 8338.8(1) | −0.6 | 0.0(5) | this work |
| form C | 8339.37(5)[b] | 0 | 2.4(5) | this work |
| R | 8339.0(1) | −0.4 | 1.1(5) | *24* |
| form L | 8339.2(2)[c] | −0.3 | 4.6(5) | this work |
| SI−CO | 8339.4(2) | 0 | 3.1(5) | this work |
| Ni($np_3$)CO | 8340.8(2) | | 8.0(5) | this work |

[a] $E_{ave}$ is the mean value of the Ni K-edge energies (8339.4 eV). [b] This value and the error represent the average of data obtained from three samples and the standard deviation, rather than the value from a summed data set and the reproducibility of that value in individual scans, which was used for other samples. [c] Because of the presence of an interfering XANES feature on the edge, the value of the edge energy was derived by fitting the edge with a combination arctangent/Gaussian function as previously described (*37*). For other samples, this procedure led to values of the edge energy that were within ±0.1 eV of the values measured directly from the spectrum.

activity or $H_2$-uptake activity before and after exposure. The first and second assays are performed to monitor the redox poise of the sample before, during, and after exposure; none of the samples exhibited a significant change in redox poise.

The XAS spectra were analyzed in analogy with previously published procedures (*32*). For the purposes of comparison, the edge energy reported in Table 1 is taken to be the energy at a normalized absorbance of 0.5, consistent with the analysis of data from *C. vinosum*, *D. gigas*, *Escherichia coli*, *T. roseopersicina*, *Desulfovibrio desulfuricans*, and *Alcaligenes eutrophus* $H_2$ase samples (*24*). The only exception to this is the reported Ni K-edge energy of form L. In this case, structure on the edge prevented a similar estimation of the edge energy, and the energy was determined by fitting the edge region with a combination arctangent/Gaussian function, as previously described (*37*). When this procedure was used on spectra from other samples, the resultant edge energy that was determined was within ±0.1 eV of that measured directly from the spectrum. For form C, data sets from three different samples were collected. The edge energy reported is the average of the three data sets, and the error reported is the standard deviation. The Ni K-edge energies and XANES data for previously published spectra of forms A, B, and R are included here for comparison with data from other forms. The areas under the peaks assigned to 1s → 3d transitions were determined by fitting a background to the region of the spectrum immediately below and above this feature in energy and integrating the difference.

EXAFS data were analyzed using the XAS analysis package WINXAS (*38*). The summed, calibrated data files were background-corrected and normalized using a two polynomial fit, with a first-order polynomial for the pre-edge region and a third-order polynomial for the post-edge region. The data were then converted to $k$ space using the relationship $[2m_e(E - E_0)/\hbar^2]^{1/2}$, where $m_e$ is the electron mass, $E$ is the photon energy, $\hbar$ is Planck's constant divided by $2\pi$, and $E_0$ is the threshold energy of the absorption edge, here defined as 8340.0 eV. Least-squares fits of the EXAFS data over a $k$ range of 2.0−14.3 Å$^{-1}$ or over the $k$ range of 2.0−12 Å$^{-1}$, where the data were limited by the presence of features associated with trace Cu in the spectrum, were performed using Fourier-filtered data with a backtransform window of 1.1−2.6 Å (uncorrected for phase shifts). Best fits were judged by minimizing GOF (*38*), GOF $= 1/\sigma^2 \sum_{i=1}^{N}[y_{exp}(i) - y_{theo}(i)]^2$ (where $N$ is the number of data points, $\sigma$ is an estimate for the experimental error, and $y_{exp}$ and $y_{theo}$ are experimental and theoretical data points, respectively) and comparing residuals (*38*) (eq 1) and the difference in the disorder parameters between the model data and the fit, $|\Delta\sigma^2| = |(\sigma_{fit}^2 - \sigma_{model}^2)|$, using the XAS formula (eq 2) (*38*), where $\sigma_{model}^2$ is the disorder parameter obtained by fitting data from the structurally characterized models used in the FEFF calculations with the calculated phase and amplitude parameters. Thus, $|\Delta\sigma^2|$ provides a comparison of the disorder in the enzyme with a well-ordered model system.

$$\text{residual}[\%] = \frac{\sum_{i=1}^{N}|y_{exp}(i) - y_{theo}(i)|}{\sum_{i=1}^{N}|y_{exp}(i)|} \cdot 100 \quad (1)$$

$$\chi(k) = \sum_j \frac{N_j S_0^2 F_j(k)}{kR_j^2} e^{(-2k^2\sigma_j^2)} e^{(-2R_j/\lambda)} \sin[2kR_j + \delta_j(k)] \quad (2)$$

Theoretical phases and amplitudes for single and multiple scattering EXAFS analyses were obtained from FEFF 6 (*39*−*41*) calculations of crystallographically characterized model compounds. The calculations included all pathways up to 6.1 Å in length. The theoretical parameters for single scattering pathways for first coordination sphere atoms, and the single scattering and the most significant multiple scattering paths for second coordination sphere atoms were then checked, using them to fit the experimental spectrum obtained for each of the model compounds. In all cases, bond lengths matching the crystallographic values within ±0.02 Å were obtained for atoms in the first and second coordination sphere of the metal. In this work, only carbonyl ligands required multiple scattering analysis. All of the calculated pathways for this ligand except the path consisting of four legs (Ni → C → Ni → C → Ni), which contributed only 4.6% of the relative intensity (all paths), were included (see supplemental Tables S9 and S10). The compounds used for the FEFF calculations were for Ni−S, tetraethylammonium tetrakis[*p*-chlorobenzenethiolatonickelate] (*42*), for Ni−O, diaqua-bis(salicylaldehydato) nickel(II) (*43*), for Ni−Fe, tris-[N,N′-dimethyl-N,N′-bis(2-mercaptoethyl)-1,3-propanediamino nickel(II)] iron(II) (*44*), and for Ni−CO, tris(2-diphenylphosphinoethyl)amino nickel(0) carbonyl, Ni($np_3$)CO (*45*). Previously published EXAFS spectra for forms A and B have been reanalyzed using this procedure and are included here for comparison between this procedure and that employed in earlier analyses and for completeness. Note that FEFF 6 calculations found no significant multiple scattering pathways (> 2.9% contribution to the spectra) mediated by the S atoms in the Ni−Fe model above either through the singly bridged Ni−Fe pair or through the doubly bridged units, and none were used in refining the Ni−Fe distance for the enzyme.

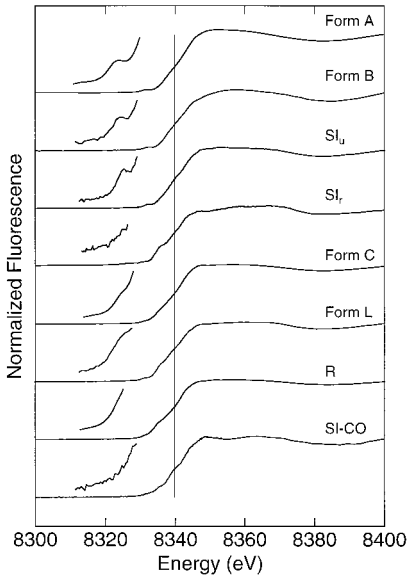


FIGURE 1: Comparison of the normalized Ni K-edge XAS spectra for samples of *C. vinosum* $H_2$ase in the edge and the XANES regions. Average Ni K-edge energy is indicated with a vertical line. Inserts are 10× expansions of the regions containing the XANES feature associated with a 1s → 3d electronic transition.

## RESULTS AND DISCUSSION

*Redox Chemistry.* Nickel K-edge XAS spectra arise from the ejection of a Ni 1s electron, which occurs near 8332 eV in Ni metal and near 8340 eV in Ni(II) coordination complexes (*46*). Since the amount of energy required to dissociate a 1s electron is sensitive to the valence electron configuration, the edge energy provides a measure of the electron density of the Ni and is therefore an indication of changes in the electron density that might arise from redox chemistry, assuming a relatively constant ligand environment. Typically, the edge energy shifts by ~2 eV with each one-electron change in oxidation state (*37*, *47*, *48*). Shifts accompanying redox processes that give rise to changes in the K-edge energy smaller than 1 eV are indicative of substantial ligand involvement in the redox process.

The XAS spectra showing the Ni K-edge region and XANES features observed for *C. vinosum* $H_2$ase are summarized in Table 1 and Figure 1. The edge energy differences measured for the *C. vinosum* $H_2$ase samples, while not large, are the largest yet observed for a [NiFe]-$H_2$ase with the exception of *A. eutrophus* $H_2$ase, in which a major change in the structure of the Ni site accompanies reductive activation (*24*, *49*). The largest difference for states related by redox chemistry is 1.6(2) eV (form B vs $SI_r$). Thus, in the absence of large changes in the ligand environment, the changes in the edge energy are consistent with both a maximal one-electron change in the Ni center and a highly covalent environment, such as the $Cys_4$ environment found in the *D. gigas* structure. The changes in edge energies are nearly twice as large as were previously observed for redox-poised samples of *T. roseopersicina* $H_2$ase (0.9(2) eV) (*32*).

The average Ni K-edge energy observed is 8339.4 eV, which coincides with the edge energy measured for form C. The samples poised in forms A, B, and $SI_u$ all have edge energies higher than this value, while the $SI_r$, form L, and R samples all have lower edge energies (Table 1). The edge energies do not vary monotonically with one-electron reductions of the enzyme (*9*, *10*, *50*), indicating that the redox status of the Ni site does not reflect the redox state of the enzyme. The edges observed for form A and form B differ by about 0.4 eV, with the B state having the higher edge energy. Reduction of form A to $SI_u$ is accompanied by a negligible (0.2 eV) change in the edge energy, similar to the form A → SI conversions reported in $H_2$ases from other sources (*24*). In contrast, reduction of form B to $SI_r$ decreases the edge energy by 1.6 eV, the largest edge energy shift observed. The Ni center in $SI_r$ is as reduced as the fully reduced form of the enzyme (R). Since $SI_u$ and $SI_r$ are both one-electron reduced states, the 1.0-eV difference between these states must be attributed to either internal redox changes, large changes in the ligand environment of the Ni center (ruled out by EXAFS analysis, vide infra), or some contribution from both.

Form C, one-electron more reduced than the SI states, has a Ni K-edge energy that lies between those measured for $SI_u$ and $SI_r$. Reduction of form C to the fully reduced state, R, leads to a decrease in the Ni K-edge energy to approximately that of $SI_r$. If one ignores forms A and $SI_u$ because they represent "unready" conformations, then the Ni K-edge energies associated with reduction of the enzyme (form B → $SI_r$ → form C → R) oscillate in the manner that would be consistent with the Ni(III) → Ni(II) → Ni(III) → Ni(II) formalism proposed by Moura and co-workers (*19*). However, such a scheme is oversimplified, since the magnitude of the changes in the edge energy between $SI_r$ and form C, and between form C and R, are less than 1 eV, indicating that either the redox changes are partially compensated for by changes in ligation of the Ni or that the redox chemistry is not centered on the Ni atom. Nonetheless, the data are consistent with models in which the active site Ni,-Fe cluster exists in two redox states, an oxidized and a reduced state, with the oxidized state accounting for all of the EPR-active species.

The photolysis of form C to form L is also accompanied by a small change in the Ni K-edge energy (−0.3 eV), indicating that the Ni center is more reduced in the photoproduct, but the change is too small to attribute to a simple reduction of the Ni center. These results are completely consistent with the previous results for the form C/form L conversion obtained using *T. roseopersicina* $H_2$-ase (*14*). The data are not consistent, however, with models wherein the Ni is reduced from Ni(III) to Ni(I) (expected edge energy shift ca. −4 eV) or where a Ni(III) center simply loses a ligand (e.g., $H^-$) because such a change would be expected to lead to an increase in the Ni K-edge energy. The data are consistent with either a structural change not involving redox chemistry or ligand dissociation at the Ni site or with changes localized on Fe or S and reflected in a small change in the Ni electron density via covalent interactions. Changes in the electron density of the Fe center are apparent from IR measurements of the intrinsic $\nu_{CO}$ frequency, which decreases by more than 50 $cm^{-1}$ upon photolysis—the largest such shift measured in the enzyme (Scheme 1) (*20*).

The role of the ligand environment in determining the Ni K-edge energy has been explored in model complexes, and it was found that changing a single hard-donor ligand with a soft-donor ligand shifts the edge energy by about −0.5 eV (*37*). These results are reflected in the Ni K-edge energy

detemined for form SI−CO, which is identical to that determined for form C. Thus, the two Ni centers have similar electron density despite the fact that one is EPR-silent and the other exhibits an S = 1/2 EPR spectrum. The results indicate that the increase in electron density expected for the conversion of form C to SI−CO (−0.6 eV by comparison with $SI_r$) is compensated for by the addition of the strong $\pi$-acid CO ligand.

*Changes in Coordination Number and Geometry.* The X-ray absorption near edge structure (XANES) in the XAS spectrum is sensitive to the number of ligands bound to the metal center and their geometry. Given the inaccuracy associated with the determination of the number of ligand donor atoms from EXAFS analysis (typically ±25% because of correlations between the number of donor atoms and the disorder in the M−L distances), XANES analysis provides the most reliable information regarding coordination number and geometry of metal centers from XAS data. The observation of XANES in the pre-edge region of the XAS spectrum is associated with high-energy electronic transitions occurring at energies less than those that produce a photoelectron. The intensity of the peak associated with a 1s → 3d electronic transition (near 8332 eV in Ni(II) complexes) is a measure of the centrosymmetry of the Ni site, since such a transition is forbidden in centrosymmetric coordination environments (e.g., octahedral and square planar environments) and gains intensity from p−d orbital mixing in noncentrosymmetric geometries (e.g., five-coordinate and tetrahedral geometries) (*33*, *37*). Studies of a number of structurally characterized Ni complexes show that small peak areas are expected for six-coordinate ($0-4 \times 10^{-2}$ eV) and planar Ni complexes ($0-3 \times 10^{-2}$ eV), intermediate areas are found for five-coordinate complexes (typically $(5-7) \times 10^{-2}$ eV), and maximum intensity is observed for tetrahedral complexes (ca. $10 \times 10^{-2}$ eV) (*37*). The high-symmetry environments may be further distinguished by the presence (square planar geometry) or absence (octahedral geometry) of a resolved peak near 8338 eV associated with a 1s → $4p_z$ electronic transition (*33*, *37*). This transition is also observed as a shoulder in the spectra of distorted planar complexes (*51*) and in spectra obtained from pyramidal five-coordinate complexes (*37*) but not in trigonal bipyramidal complexes (*37*).

None of the spectra shown in Figure 1 exhibit a resolved maximum corresponding to the 1s → $4p_z$ electronic excitation (with shakedown contributions), ruling out a four-coordinate planar geometry for the Ni site in any of these states. However, the spectra for $SI_r$, SI−CO, L and R reveal shoulders that can be assigned to this transition in a four-coordinate distorted planar or five-coordinate pyramidal geometry. The intensities (areas) measured for the 1s → 3d transition fall into two groups (Table 1 and Figure 1). Forms A/B and $SI_u$ have peaks with areas in the $5-7 \times 10^{-2}$ eV range that are indicative of five-coordinate Ni sites; this result is consistent with the five-coordinate environment found for the Ni site in the *D. gigas* $H_2$ase crystal structure. The $SI_r$, SI−CO, forms C and R states have small 1s → 3d peak areas. The value for form L lies between those that are typical of octahedral and five-coordinate geometries, suggesting a highly distorted six-coordinate structure. On the basis of the XANES analysis, four-coordinate planar Ni sites and tetrahedral Ni sites are ruled out for all of the forms. Forms A, B, and $SI_u$ are clearly five-coordinate, and the data for form C are most consistent with a six-coordinate site (small 1s → 3d peak + absence of any shoulder for a 1s → $4p_z$ transition). For the remaining samples, $SI_r$, SI−CO, forms C and R, the low 1s → 3d intensity rules out a five-coordinate geometry, and the observation of a shoulder attributable to a 1s → $4p_z$ transition indicates a distorted planar configuration. In the case of SI−CO, the geometry/coordination number suggest that either CO is not bound to the Ni or that the CO displaces one of the protein ligands to retain the four-coordinate structure.

Combining the results from XANES and K-edge energy analysis, the reduction of form A to $SI_u$ appears to involve a small increase in electron density at Ni with no change in coordination geometry. In contrast, the form B → $SI_r$ conversion involves a change in coordination number from five to four accompanied by the largest increase in electron density between two states (1.6 eV decrease in edge energy). The $SI_u$ → $SI_r$ conversion follows a pattern similar to the form B → $SI_r$ conversion, with a decrease in coordination geometry (five to four) and an increase (1 eV) in electron density. This conversion occurs between two states at the same redox level, strongly suggesting that internal changes in electron density (internal redox) are involved to account for the increase in electron density observed. For the remaining active forms, the conversion of $SI_r$ → form C → R is consistent with a change in coordination number of 4 → 6 → 4, in combination with edge energy shifts that correspond in direction (but not in magnitude) with Ni(II) → Ni(III) → Ni(II) redox chemistry. The trend is opposite to the one expected for simple ligand addition and dissociation to Ni(II), and so to an extent (ca. 1 eV based on model studies) the change in coordination number moderates the electron density changes associated with the redox process. The changes observed are consistent with the tendency of four-coordinate Ni(II) coordination complexes to gain ligands upon oxidation to Ni(III) (*52*−*54*).

*The Ligand Environment.* The post-edge XANES is sensitive to the types of ligand donor atoms present in the primary Ni coordination sphere and their spatial arrangement, thus providing a sensitive fingerprint for comparing samples. None of the samples show a significant white line (a quasiatomic transition just above the edge in energy, Figure 1), an observation that is consistent with a predominantly S-rich ligand environment in all states (*33*, *37*). The ligands bound to Ni and the structural differences in the Ni sites can be examined in detail by measuring the effect on the X-ray absorption coefficient of the scattering of a photoelectron generated by dissociation of a Ni 1s electron. The resulting extended X-ray absorption fine structure (EXAFS) can be analyzed to provide local structural information regarding the Ni sites. In addition to providing a "best fit" structure for the Ni site consistent with the EXAFS spectra from the samples, the analyses reported in Table 2 and summarized in Table 3 were designed specifically to test for the presence of a low Z bridge, for structural changes that result in different Ni−S distances in the primary coordination sphere, and to look for changes in the Ni−Fe distance and for the presence of CO in the primary coordination sphere of Ni in SI−CO. Thus, Table 2 contains, for each sample, the best single shell fit (based on the lowest value of the GOF criterion and the lowest value of $\Delta\sigma^2$),

Table 2: Selected Curve-Fitting of Filtered EXAFS Spectra for *Chromatium vinosum* Hydrogenase[a]

| sample/FT limit (Å$^{-1}$) | fit | *N* Ni−X | *R* (Å) | $\sigma^2$ (× 10$^3$ Å)[b] | $\Delta\sigma^2$ (× 10$^3$ Å) | GOF | sample/FT limit (Å$^{-1}$) | fit | *N* Ni−X | *R* (Å) | $\sigma^2$ (× 10$^3$ Å) | $\Delta\sigma^2$ (× 10$^3$ Å) | GOF |
|---|---|---|---|---|---|---|---|---|---|---|---|---|---|
| form A | A01 | 4 Ni−S | 2.1710(1) | *12.3* | 9.8 | 16.9 | form C | C01 | 4 Ni−S | 2.2212(3) | 7.3 | 4.8 | 30.8 |
| $k = 2-12$ | A02 | 4 Ni−S | 2.1691(1) | *12.0* | 9.5 | 14.5 | $k = 2-14.3$ | C02 | 4 Ni−S | 2.2070(3) | 6.9 | 4.4 | 18.2 |
| | | 1 Ni−Fe | 2.6324(1) | *19.2* | 17.7 | | | | 1 Ni−Fe | 2.5522(5) | 4.0 | 2.5 | |
| | A03 | 1 Ni−O | 1.8908(1) | 3.1 | −1.5 | 5.2 | | C03 | 2 Ni−O | 2.0671(5) | 0.6 | −4.0 | 28.0 |
| | | 3 Ni−S | 2.1932(1) | *10.5* | 8.0 | | | | 4 Ni−S | 2.1899(5) | *11.3* | 8.8 | |
| | A04 | 3 Ni−S | 2.1331(1) | 8.4 | 5.9 | 10.6 | | C04 | 3 Ni−S | 2.1974(3) | 1.5 | −1.0 | 20.3 |
| | | 2 Ni−S | 2.2871(1) | 8.8 | 6.3 | | | | 2 Ni−S | 2.3536(4) | 0.5 | −2.0 | |
| | A05 | 1 Ni−O | 1.8724(1) | 1.6 | −3.0 | 4.1 | | C05 | 2 Ni−S | 2.1922(3) | 0.4 | −2.1 | 12.2 |
| | | 2 Ni−S | 2.1790(1) | 5.5 | 3.0 | | | | 2 Ni−S | 2.378(1) | 5.3 | 2.8 | |
| | | 1 Ni−S | 2.3070(2) | *10.4* | 7.9 | | | | 1 Ni−Fe | 2.491(1) | 2.3 | 0.8 | |
| form B | B01 | 4 Ni−S | 2.2180(1) | *10.6* | 8.1 | 22.2 | form L | L01 | 4 Ni−S | 2.2352(1) | 7.7 | 5.2 | 15.4 |
| $k = 2-12$ | B02 | 4 Ni−S | 2.2189(1) | *10.7* | 8.2 | 14.2 | $k = 2-14.3$ | L02 | 4 Ni−S | 2.2249(1) | 8.1 | 5.6 | 7.2 |
| | | 1 Ni−Fe | 2.8549(1) | *10.8* | 9.3 | | | | 1 Ni−Fe | 2.5603(1) | 7.9 | 6.4 | |
| | B03 | 1 Ni−O | 1.8606(1) | 2.2 | −2.4 | 11.9 | | L03 | 1 Ni−O | 1.9697(6) | *12.5* | 7.9 | 15.7 |
| | | 3 Ni−S | 2.2314(1) | 6.7 | 4.2 | | | | 3 Ni−S | 2.2371(1) | 5.8 | 3.3 | |
| | B04 | 2 Ni−S | 2.1084(1) | 7.3 | 4.8 | 15.4 | | L04 | 3 Ni−S | 2.2109(1) | 4.0 | 1.5 | 14.7 |
| | | 3 Ni−S | 2.2652(1) | 5.4 | 2.9 | | | | 1 Ni−S | 2.3471(1) | 0.5 | −2.0 | |
| | B05 | 1 Ni−O | 1.8436(1) | 3.5 | −1.1 | 4.9 | form R | R01 | 4 Ni−S | 2.2004(2) | 7.2 | 4.7 | 22.5 |
| | | 4 Ni−S | 2.2318(1) | 9.6 | 7.1 | | $k = 2-14.3$ | R02 | 4 Ni−S | 2.1895(2) | 7.0 | 4.5 | 12.4 |
| | | 1 Ni−Fe | 2.8412(1) | *11.6* | 10.1 | | | | 1 Ni−Fe | 2.5354(3) | 5.1 | 3.6 | |
| form SI$_u$ | SU01 | 4 Ni−S | 2.2159(1) | 8.8 | 6.3 | 29.7 | | R03 | 2 Ni−O | 1.949(1) | *14.9* | 10.3 | 21.4 |
| $k = 2-14.3$ | SU02 | 4 Ni−S | 2.2125(1) | 9.3 | 6.8 | 29.2 | | | 2 Ni−S | 2.1984(2) | 2.6 | 0.1 | |
| | | 1 Ni−Fe | 2.523(1) | *19.3* | 17.8 | | | R04 | 2 Ni−S | 2.1597(2) | 1.2 | −1.3 | 23.5 |
| | SU03 | 2 Ni−O | 1.9073(1) | 2.9 | −1.7 | 10.8 | | | 2 Ni−S | 2.2904(3) | 2.3 | −0.2 | |
| | | 3 Ni−S | 2.2398(1) | 5.4 | 2.9 | | form SI−CO | CO01 | 4 Ni−S | 2.2770(2) | 7.3 | 4.8 | 20.2 |
| | SU04 | 1 Ni−S | 2.0525(2) | 2.5 | 0 | 20.5 | $k = 2-14.3$ | CO02 | 4 Ni−S | 2.2698(3) | 8.5 | 6.0 | 13.0 |
| | | 5 Ni−S | 2.2288(1) | 7.5 | 5.0 | | | | 1 Ni−Fe | 2.550(1) | *10.2* | 8.7 | |
| | SU05 | 2 Ni−O | 1.9119(1) | 1.3 | −3.3 | 7.1 | | CO03 | 1 Ni−C | 1.7948(8) | 4.5 | −0.6 | 15.6 |
| | | 2 Ni−S | 2.2273(1) | 1.2 | −1.3 | | | | 4 Ni−S | 2.2737(2) | 7.5 | 5.0 | |
| | | 1 Ni−S | 2.3635(4) | 4.3 | 1.8 | | | CO04 | 2 Ni−S | 2.2148(3) | 2.0 | −0.5 | 14.5 |
| form SI$_r$ | SR01 | 4 Ni−S | 2.2335(4) | *17.0* | 14.5 | 23.8 | | | 2 Ni−S | 2.3448(3) | 1.2 | −1.3 | |
| $k = 2-12$ | SR02 | 4 Ni−S | 2.2155(4) | *18.4* | 15.9 | 14.2 | | CO05 | 1 Ni−C | 1.7946(8) | 4.1 | −1.0 | 7.3 |
| | | 1 Ni−Fe | 2.600(1) | *13.9* | 12.4 | | | | 4 Ni−S | 2.2640(3) | 8.8 | 6.3 | |
| | SR03 | 1 Ni−O | 1.884(1) | 9.8 | 5.2 | 21.7 | | | 1 Ni−Fe | 2.554(1) | 9.6 | 8.1 | |
| | | 3 Ni−S | 2.2530(4) | *13.7* | 11.2 | | | CO06 | 1 Ni−C | 1.7821(8) | 4.2 | −0.9 | 5.6 |
| | SR04 | 2 Ni−S | 2.1590(4) | 6.4 | 3.9 | 14.3 | | | 1 Ni−O | 2.898(1) | 4.4 | −1.0 | |
| | | 2 Ni−S | 2.3352(4) | 5.3 | 2.8 | | | | 3 Ni−S | 2.2546(3) | 6.9 | 4.4 | |
| | SR05 | 2 Ni−S | 2.1601(6) | 8.7 | 6.2 | 11.1 | | | 1Ni−Fe | 2.5398(7) | 5.4 | 3.9 | |
| | | 2 Ni−S | 2.335(1) | 9.4 | 6.9 | | | | | | | | |
| | | 1 Ni−Fe | 2.558(3) | *17.1* | 15.6 | | | | | | | | |

[a] X is the scattering atom for each shell; *R* is the Ni−X distance; $\sigma^2$ is the root-mean-square disorder in the Ni−X distance; $\Delta\sigma^2$ is $\sigma^2$ relative to calculated values for reference compounds; GOF is the goodness-of-fit defined in Experimental Procedures. The accuracies of distances determined by EXAFS for atoms in the first coordination sphere of the metal are limited to ±0.02 Å by the theoretical phase parameters. The refinements generally show precisions that are less than 0.02 Å for well-ordered shells, thus differences in distances between samples using equivalent fits are more accurate than the absolute distances. [b] Italicized values are approaching physical insignificance. Large values of $\sigma^2$ suggest that the shell involved has a coordination number that is too large or is badly disordered and may be unnecessary for fitting the data.

the best two shell fits involving one or two low Z atoms, the best two shell fit resulting from two shells of S scattering atoms, the best two shell fit including a Ni−Fe vector, and the best overall three shell fit. The data and the overall best fit for each sample are illustrated in Figures 2 and 3. Previous analyses of data from *C. vinosum* $H_2$ase and other $H_2$ases were limited to a maximum value of $k = 12-12.5$ Å$^{-1}$ because of the presence of trace Cu in the samples (*24*). These data were used in the new refinements presented here for forms A and B and are included here for comparison between fitting procedures and for completeness. The sample of SI$_r$ analyzed here for the first time also contained trace Cu, and the analysis was therefore limited to $k = 12$ Å$^{-1}$. The data presented here for *C. vinosum* samples in forms SI−CO, C, L, and R did not contain features associated with trace Cu, and in these cases it has been possible to extend the data analysis to $k = 14.3$ Å$^{-1}$, increasing the sensitivity to scattering from the Fe atom in the active site and aiding in distinguishing it from S-scattering atoms at long distances (≥2.5 Å).

All of the single shell fits show a preference for S-donor ligands over N/O donor ligands, consistent with a predominantly S-donor ligand environment in all cases. The GOF values that are observed for fits involving a single shell of S scattering atoms are in general large and not very sensitive to the number of S atoms in the primary coordination sphere. This is because a single shell does not adequately fit the data, and the number of S atoms is correlated with the value of $\sigma^2$, which is a measure of the disorder of the Ni−S bond lengths. Dynamic disorder is minimized by taking spectra on samples held at low temperature (50 K in this study). However, static differences in the Ni−S distances can still occur, and thus, four well-ordered Ni−S distances can give a similar EXAFS amplitude as six less well-ordered Ni−S distances. This correlation effectively limits the accuracy of the determination of the number of scattering atoms in a refined shell to ca. ±25% or about ±1 donor atom. To minimize the correlation of *N* and $\sigma^2$, the fitting strategy held the number of scattering atoms (*N*) to integer values and varied $\sigma^2$ to obtain the best fit of the amplitude (*55*).

Table 3: Summary of EXAFS Fitting Results for *Chromatium vinosum* Hydrogenase

| sample/ FT limits (Å$^{-1}$) | short Ni−X (Å)[a] (X = C, N, or O) | ave Ni−S (Å)[b] | split S shell[c] | Ni−Fe (Å) |
|---|---|---|---|---|
| A ($k$ = 2−12) | Ni−O = 1.91(2) | 2.17(2) | yes (0.16) | nd[d] |
| B ($k$ = 2−12) | Ni−O = 1.86(2) | 2.22(2) | yes (0.14) | 2.86(2) |
| $SI_u$ ($k$ = 2−14.3) | Ni−O = 1.91(2) | 2.20(2) | yes (0.17) | nd |
| $SI_r$ ($k$ = 2−12) | none | 2.23(2) | yes (0.18) | 2.60(2) |
| C ($k$ = 2−14.3) | none | 2.22(2) | yes (0.15) | 2.49(2) |
| L ($k$ = 2−14.3) | none | 2.24(2) | yes (0.13) | 2.56(2) |
| R ($k$ = 2−14.3) | none | 2.20(2) | no | 2.54(2) |
| SI−CO ($k$ = 2−14.3) | Ni−C =1.78(2) | 2.28(2) | yes (0.13) | 2.55(2) |

[a] In cases where a shell of O coordination is indicated, the bond length is given in parentheses. A blank indicates that the fit is not significantly improved by the addition of a short O/N scattering atom. [b] The average Ni−S distances were taken from the single shell fits.[c] If the fit is improved by using two S shells, the difference in the Ni−S distances obtained in the fit is indicated in parentheses. [d] Not determined.

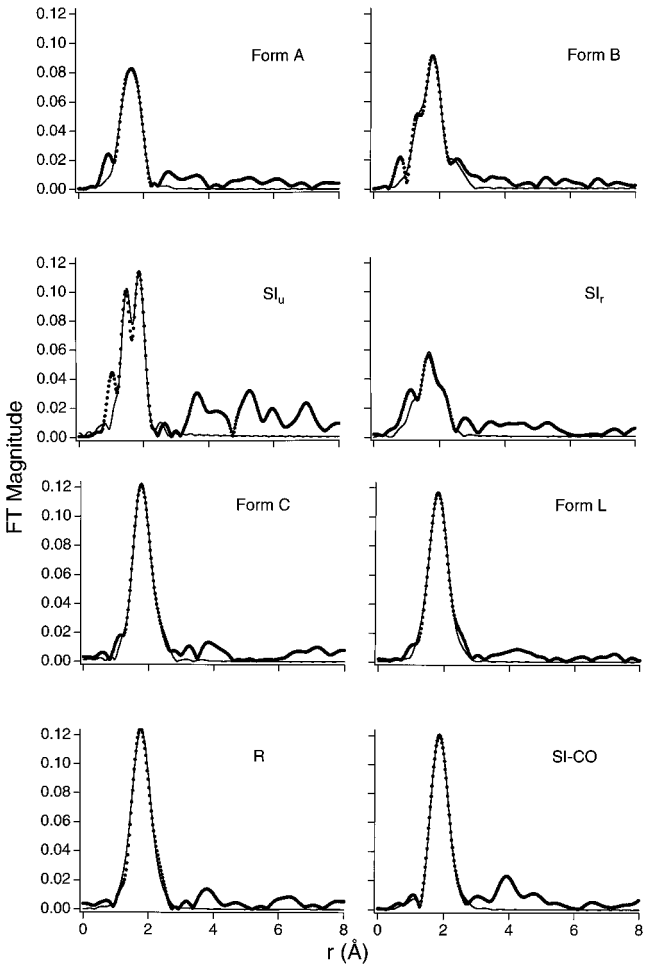


FIGURE 2: A comparison of the Fourier-transformed ($k$ = 2−12 Å$^{-1}$ for forms A, B, and $SI_r$; $k$ = 2−14.3 Å$^{-1}$ for $SI_u$, forms C, R, L, and SI−CO) Ni K-edge EXAFS data (solid circles), fits (solid lines) from *C. vinosum* $H_2$ase. Fits shown are A05, B05, SU05, SR05, C05, R02, L02, and CO06 from Table 2.

The addition of a shell of O scattering atoms to a single shell of S scattering atoms was used to test for the presence

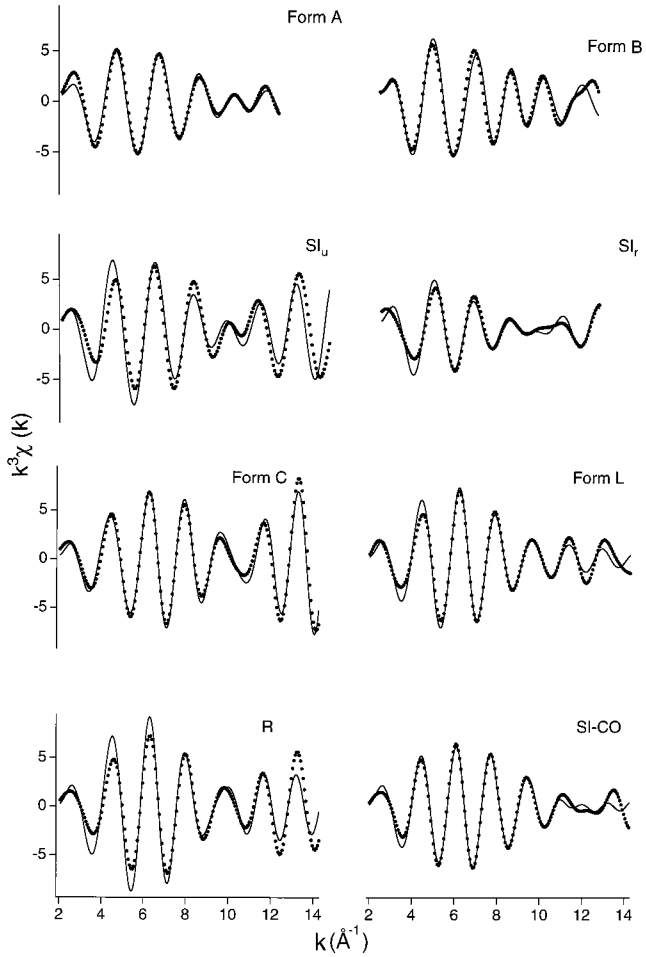


FIGURE 3: Fourier-filtered (backtransform window = 1.1−2.6 Å, uncorrected for phase shifts) EXAFS data (solid circles) and fits (solid lines) of forms A, B, $SI_u$ $SI_r$, C, R, L, and SI−CO. Fits shown are given in the caption for Figure 2.

of a low Z scattering atom in the primary coordination sphere of the Ni (Tables 2 and 3). For forms A, B, $SI_u$, and SI−CO, two shell fits incorporating a short Ni−X bond improved the fit. The two best fits for form A (Table 2, A03 and A05) indicate a Ni−O vector at 1.91(2) Å. This is longer than would be expected for the Ni-oxo bridge predicted by the 1.7 Å distance in the *D. gigas* crystal structure (*17*) and is more consistent with a hydroxo bridge. An O-donor is also supported from the observation of $^{17}O$ hyperfine interactions in the EPR spectra of forms A and B obtained after reoxidation of reduced enzyme with $^{17}O_2$ (*6*). The fits for form B and $SI_u$ were also improved by the addition of a shell of short oxygen atoms at 1.86(2) and 1.91 Å, respectively (Table 2, B03, B05, SU03 and SU05). $SI_r$ is the first form in the reductive activation of the enzyme in which the fit is not improved by the addition of a shell of O atoms at a distance of ∼1.9 Å (Table 2, SR03). This is consistent with the XANES analysis, which shows a change in coordination number from five in forms A, B, and $SI_u$ to four in $SI_r$ and can be assigned to the loss of an O-donor ligand on the basis of the EXAFS analysis. None of the samples in which the enzyme is more reduced than the SI level show any evidence of a short Ni−O bond, consistent with the findings from the crystal structure of reduced *D. baculatum* $H_2$ase, which shows a similar structure to the oxidized *D. gigas* enzyme but lacks a bridging low Z atom

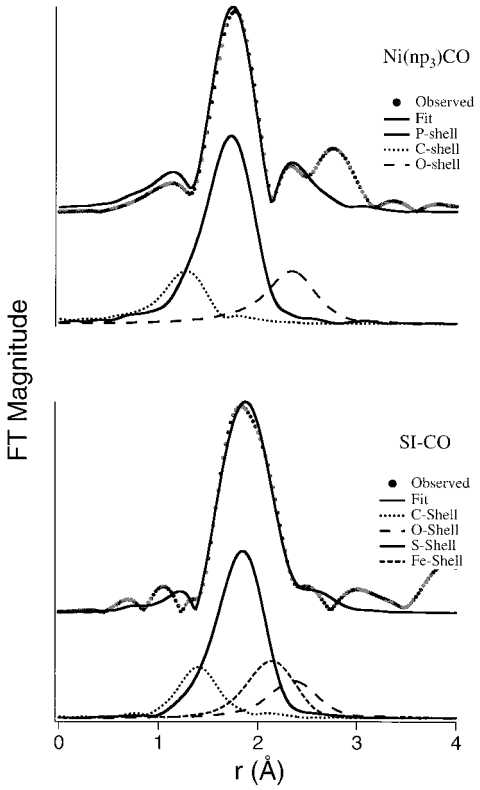


FIGURE 4: Comparison of the deconvoluted Fourier-transformed ($k = 2-13$ Å$^{-1}$ for Ni(np$_3$)CO; $k = 2-14.3$ Å$^{-1}$ for SI−CO) Ni K-edge EXAFS data (solid circles) and fits (solid lines) for Ni-(np3)CO (upper spectrum) and *C. vinosum* $H_2$ase form SI−CO. Distances ($r$) are uncorrected for phase shifts. The lower part of each FT spectrum shows the contribution from each component of the fit to the overall fit of the FT spectrum.

(*56*). The data presented here show that the loss of the bridging hydroxo/oxo ligand is a feature of reductive activation of the enzyme that occurs upon conversion to SI$_r$.

The fit for SI−CO also shows significant improvement when a low Z atom is added (CO03, CO05, and CO06). The refined distance (1.81 Å) is the shortest distance observed for all of the two shell fits, suggesting that the ligand involved in this case is CO rather than a ligand derived from water. Although C atom scattering parameters fit the data for SI−CO better than O atom parameters, and the opposite is true for form A, the inability to clearly distinguish two atoms with similar electron density makes it impossible to assign this to a Ni−CO ligand on the basis of the analysis of atoms in the first coordination sphere of the Ni. To unambiguously assign the CO ligand, multiple scattering analysis was employed to fit scattering from the second coordination sphere O atom of the CO ligand. FEFF 6 (*39*−*41*) was used to calculate the EXAFS spectrum of the crystallographically characterized model compound tris[2-(diphenylphosphinoethyl)amine]Ni(II)carbonyl, Ni(np$_3$)CO (*45*), to obtain parameters for a Ni−CO interaction. The parameters obtained were checked by using them to analyze experimental data obtained from the model compound. The results of these fits are summarized in Figure 4 and in Table 4, which also shows the distances obtained from EXAFS analysis in comparison with the crystallographic distances. Addition of a Ni−CO interaction to the fit of the SI−CO data improved the fit significantly (Table 2, CO06). The Ni−C distance refined to 1.78(2) Å, and the Ni−O distance refined to 2.90(2) Å,

Table 4: Curve-Fitting of Filtered EXAFS Spectra for Ni(np$_3$)CO

| $N$ Ni−X | $R$ (Å) | $\sigma^2$ ($\times 10^3$ Å) | $\Delta\sigma^2$ ($\times 10^3$ Å)[a] | GOF | ave crystallogr dist (*45*) |
|---|---|---|---|---|---|
| 3 Ni−P | 2.2013(1) | 5.3 | 2.4 | 28.1 | |
| 3 Ni−P | 2.1940(1) | 5.3 | 2.4 | 19.1 | |
| 1 Ni−C | 1.7222(2) | 2.3 | −2.8 | | |
| 3 Ni−P | 2.1945(1) | 5.5 | 2.6 | 9.2 | 2.22(1) |
| 1 Ni−C | 1.7200(2) | 2.6 | −2.1 | | 1.74(2) |
| 1 Ni−O | 2.8842(2) | 3.2 | −2.2 | | 2.92(4)[b] |

[a] In the case of this model system, $\Delta\sigma^2$ represents the difference between the $\sigma^2$ value obtained from the FEFF calculation and the value obtained from fitting experimental data for this complex using the calculated amplitude and phase parameters. [b] Distances to second coordination sphere atoms determined from EXAFS analysis generally agree with crystallographic distances to within ±0.02 Å; however, the crystallographically determined Ni−O distance for the Ni−CO ligand in the model compound has a large error. The EXAFS value determined is within the crystallographic error.

leading to a C−O bond length of 1.12(4) Å. Although this is short for a C−O bond, it is not without precedent for Ni−CO complexes (*57*−*60*) and indicates that the CO is approximately linear and a terminal ligand of the Ni center.

The CO parameters were also checked against data from form A, which has a short bond involving a low-Z scattering atom that is not due to the presence of CO. The data were unable to accommodate the inclusion of a CO ligand, demonstrating that the two Ni ligand environments can be confidently distinguished.

Another feature of the Ni ligand environment in the structure of the active site of *D. gigas* $H_2$ase is two very different Ni−S distances for the terminal (2.2 and 2.3 Å) and bridging cysteinate ligands (2.6 Å), which average 2.4 Å and differ by over 0.3 Å. The average Ni−S distance determined from EXAFS analysis is 2.17(2)−2.23(2) Å for all of the forms of *C. vinosum* $H_2$ase that are related by redox processes (Table 3), demonstrating that the Ni−S bond is not very sensitive to the redox status of the enzyme, as noted in previous studies (*24*, *32*). The largest average Ni−S distance observed, and the only one that is truly distinct, is found in SI−CO (2.28 Å) (Table 3). The shortest average Ni−S distance for *C. vinosum* $H_2$ase, found in form A (2.17 Å), is the same average Ni−S distance obtained from EXAFS analysis of *D. gigas* $H_2$ase in form A (*24*). To examine the possibility that two shells of S-donor ligands at distinct distances exist, the single shell of Ni−S scattering atoms was split into two shells and refined separately. Splitting the two Ni−S shells leads to improved fits for all forms except the fully reduced form, R (Tables 2 and 3). However, in several cases (e.g., forms B and L), the improvement in the GOF value is not enough to justify the additional parameters. Nonetheless, the difference between the two shells of S scattering atoms obtained by modeling the S environment with two shells is very consistent between the samples (0.16-(3) Å, Table 3) and indicates that the spread of Ni−S distances in this active site must be considerably less than seen in the crystal structure of the *D. gigas* enzyme.

The addition of an Fe scattering atom to a single shell of S atoms improves the fits significantly for forms B, SI$_r$, SI−CO, C, L, and R (Table 2) but not for forms A and SI$_u$. In form B, the Ni−Fe distance obtained is longer than that in the other forms [2.85(5) Å] and indistinguishable from the value found in the *D. gigas* $H_2$ase crystal structure involving

Scheme 2

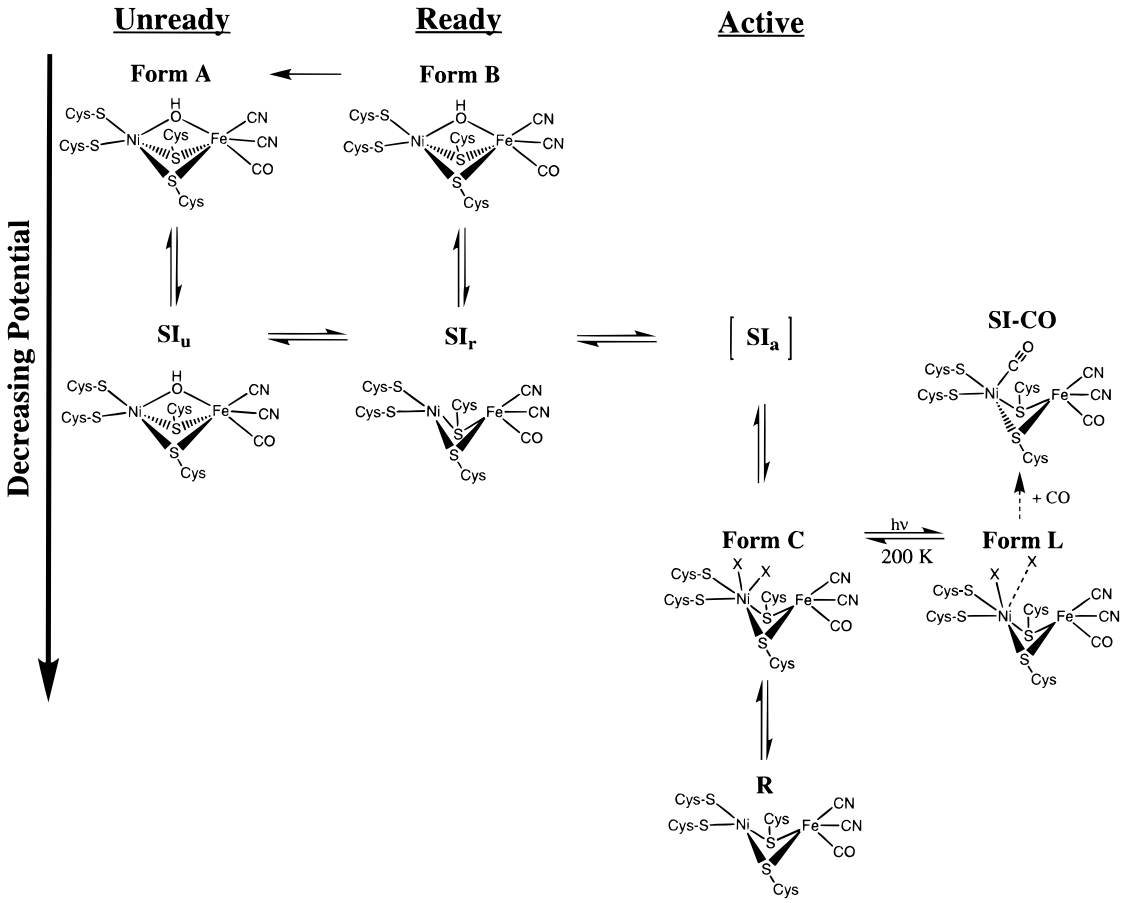


oxidized enzyme (2.9 Å) (*17*). The distances found in the other forms of the enzyme are 2.5−2.6 Å (Table 3) and are comparable to that found in the *D. baculatum* $H_2$ase crystal structure involving reduced enzyme (2.5 Å) (*56*). The data presented here establish that the shortening of the Ni−Fe distance is also a feature of reductive activation of the enzyme and occurs at the SI redox level.

The EXAFS fits for forms C and L feature a lower number of scattering atoms (4) than predicted from the XANES analysis (6). This could arise from the presence of hydrogen ligands, which would not have sufficient electron density to give rise to significant backscattering, or from disordered protein or water ligands. The possibility of ligation by ligands derived from water is suggested by ENDOR measurements that demonstrate that solvent can access the active site in form C (*61*).

The structures that emerge from EXAFS analysis of SI−CO complex and form L show that these structures, which are not natural intermediates, are very similar to those found in other forms of the enzyme. The addition of CO to the active site does not perturb the overall structure dramatically, although this structure leads to slightly longer Ni−S distances than in the other forms, and XANES analysis suggests the possible loss of one cysteinate ligand. The Ni−Fe distance is essentially identical to those found for reduced enzyme samples. In the case of form L, the similarity of the Ni−S distances and the Ni−Fe distance to those found for form C provide no support for the Ni-based redox chemistry suggested earlier by one of our laboratories (*15*) or for ligand dissociations during the photoprocess, although there appears to be a trend toward a either a distorted six-coordinate or five-coordinate structure from XANES analysis in both this enzyme and in the $H_2$ase from *T. roseopersicina* (*24*).

## CONCLUSIONS

The results of the analysis of the XAS spectra obtained for samples of *C. vinosum* $H_2$ase poised in eight distinct states lead to the following conclusions, which are summarized in Scheme 2.

(i) Ni K-edge energy analysis shows that the reduction of the enzyme and the formal redox state of the Ni atom are not correlated. Instead, the formal redox state of the Ni center appears to oscillate between Ni(III) in all of the EPR-active states and Ni(II) in all of the EPR-silent states. The changes in the Ni K-edge energy associated with the form B → SI$_r$ conversion is large enough to account for a one-electron redox state change in a Ni center in a covalent ligand environment. The magnitude of the Ni K-edge energy change associated with the SI$_r$ → form C reduction is in the correct direction but is of insufficient magnitude to be a simple reoxidation of the Ni center. However, if the effects of the geometry/coordination number change accompanying this conversion (4 → 6) detected by XANES analysis are factored in, this transition and the subsequent reduction of form C → R are also of sufficient magnitude to account for one-electron redox state changes in the Ni center.

(ii) The short Ni−O bond that is a feature of oxidized enzyme (forms A and B) and the unready EPR-silent intermediate (SI$_u$) is lost upon conversion to SI$_r$. This result

establishes that this structural change is a feature of the reductive activation of the enzyme and occurs upon conversion to $SI_r$.

(iii) The difference in the Ni−S distances between terminal and bridging thiolate ligands is considerably less than the spread of Ni−S distances observed in the *D. gigas* hydrogenase crystal structure.

(iv) A shortening of the Ni−Fe distance from 2.85(2) to 2.5−2.6 Å is also a feature of the reductive activation of the enzyme and also occurs at the SI level. Thus, the change in the Ni−Fe distance appears to be associated with the loss of the O-bridging ligand rather than with the presence of a bridging hydride.

## SUPPORTING INFORMATION AVAILABLE

Tables S1−S8 of fits of Ni K-edge Fourier-filtered EXAFS data for the hydrogenase samples featured in this paper and Tables S9−S10 of FEFF 6 pathways used in fitting the data. This material is available free of charge via the Internet at http://pubs.acs.org.

## REFERENCES


1. Hausinger, R. P. (1987) *Microbiol. Rev. 51*, 22−42.
2. Przybyla, A. E., Robbins, J., Menon, N., and Peck, H. D. J. (1992) *FEMS Microbiol. Rev. 88*, 109−135.
3. Albracht, S. P. J. (1994) *Biochim. Biophys. Acta 1188*, 167−204.
4. Adams, M. W. W. (1990) *Biochim. Biophys. Acta 1020*, 115−145.
5. Thauer, R. K., Klein, A. R., and Hartmann, G. C. (1996) *Chem. Rev. 96*, 3031−3042.
6. Van der Zwaan, J. W., Coremans, J. M. C. C., Bouwens, E. C. M., and Albracht, S. P. J. (1990) *Biochim. Biophys. Acta 1041*, 101−110.
7. Surerus, K. K., Chen, M., van der Zwaan, J. W., Rusnak, F. M., Kolk, M., Duin, E. C., Albracht, S. P. J., and Muenck, E. (1994) *Biochemistry 33*, 4980−4993.
8. Hausinger, R. P. (1993) *Biochemistry of Nickel*, Vol. 12, Plenum Press, New York.
9. Roberts, L. M., and Lindahl, P. A. (1995) *J. Am. Chem. Soc. 117*, 2565−2572.
10. Coremans, J. M. C. C., Van Garderen, C. J., and Albracht, S. P. J. (1992) *Biochim. Biophys. Acta 1119*, 148−156.
11. de Lacey, A. L., Hatchikian, E. C., Volbeda, A., Frey, M., Fontecilla-Camps, J. C., and Fernandez, V. M. (1997) *J. Am. Chem. Soc. 119*, 7181−7189.
12. Coremans, J. M. C. C., Van der Zwaan, J. W., and Albracht, S. P. J. (1992) *Biochim. Biophys. Acta 1119*, 157−168.
13. Van der Zwaan, J. W., Albracht, S. P. J., Fontijn, R. D., and Slater, E. C. (1985) *FEBS Lett. 179*, 271−277.
14. Whitehead, J. P., Gurbiel, R. J., Bagyinka, C., Hoffman, B. M., and Maroney, M. J. (1993) *J. Am. Chem. Soc. 115*, 5629−5635.
15. Happe, R. P., Roseboom, W., and Albracht, S. P. J. (1999) *Eur. J. Biochem. 259*, 602−608.
16. Volbeda, A., Charon, M. H., Piras, C., Hatchikian, E. C., Frey, M., and Fontecilla-Camps, J. C. (1995) *Nature 373*, 580−587.
17. Volbeda, A., Garcin, E., Piras, C., de Lacey, A. L., Fernandez, V. M., Hatchikian, E. C., Frey, M., and Fontecilla-Camps, J. C. (1996) *J. Am. Chem. Soc. 118*, 12989−12996.
18. Frey, M. (1998) *Struct. Bonding 90* (Metal Sites in Proteins and Models: Redox Centres), 98−126.
19. Moura, J. J. G., Teixeira, M., Moura, I., and LeGall, J. (1988) in *The Bioinorganic Chemistry of Nickel* (Lancaster, J. R., Jr., Ed.) pp 191−226, VCH, New York.
20. Bagley, K. A., Duin, E. C., Roseboom, W., Albracht, S. P. J., and Woodruff, W. H. (1995) *Biochemistry 34*, 5527−5535.
21. Bagley, K. A., Van Garderen, C. J., Chen, M., Woodruff, W. H., Duin, E. C., and Albracht, S. P. J. (1994) *Biochemistry 33*, 9229−9236.
22. Van der Spek, T. M., Arendsen, A. F., Happe, R. P., Yun, S., Bagley, K. A., Stufkens, D. J., Hagen, W. R., and Albracht, S. P. J. (1996) *Eur. J. Biochem. 237*, 629−634.
23. Teixeira, M., Moura, I., Xavier, A. V., Moura, J. J. G., LeGall, J., DerVartanian, D. V., Peck, H. D., Jr., and Huynh, B.-H. (1989) *J. Biol. Chem. 264*, 16435−16450.
24. Gu, Z., Dong, J., Allan, C. B., Choudhury, S. B., Franco, R., Moura, J. J. G., Moura, I., LeGall, J., Przybyla, A. E., Roseboom, W., Albracht, S. P. J., Axley, M. J., Scott, R. A., and Maroney, M. J. (1996) *J. Am. Chem. Soc. 118*, 11155−11165.
25. Happe, R. P., Roseboom, W., Pierik, A., Albracht, S. P. J., and Bagley, K. A. (1997) *Nature 385*, 126.
26. Pierik, A. J., Roseboom, W., Happe, R. P., Bagley, K. A., and Albracht, S. P. J. (1999) *J. Biol. Chem. 274*, 3331−3337.
27. Lai, C.-H., Lee, W.-Z., Miller, M. L., Reibenspies, J. H., Darensbourg, D. J., and Darensbourg, M. Y. (1998) *J. Am. Chem. Soc. 120*, 10103−10114.
28. Huyett, J. E., Carepo, M., Pamplona, A., Franco, R., Moura, I., Moura, J. J. G., and Hoffman, B. M. (1997) *J. Am. Chem. Soc. 119*, 9291−9292.
29. Dole, F., Fournel, A., Magro, V., Hatchikian, E. C., Bertrand, P., and Guigliarelli, B. (1997) *Biochemistry 36*, 7847−7854.
30. Lindahl, P. A., Kojima, N., Hausinger, R. P., Fox, J. A., Teo, B. K., Walsh, C. T., and Orme-Johnson, W. H. (1984) *J. Am. Chem. Soc. 106*, 3062−3064.
31. Scott, R. A., Wallin, S. A., Czechowski, M., DerVartanian, D. V., LeGall, J., Peck, H. D., Jr., and Moura, I. (1984) *J. Am. Chem. Soc. 106*, 6864−6865.
32. Bagyinka, C., Whitehead, J. P., and Maroney, M. J. (1993) *J. Am. Chem. Soc. 115*, 3576−3585.
33. Eidsness, M. K., Sullivan, R. J., and Scott, R. A. (1988) in *The Bioinorganic Chemistry of Nickel* (Lancaster, J. R., Jr., Ed.) pp 73−91, VCH, New York.
34. Muller, J. G., Hickerson, R. P., Perez, R. J., and Burrows, C. J. (1997) *J. Am. Chem. Soc. 119*, 1501−1506.
35. Cramer, S. P., Ralston, C. Y., Wang, H., and Bryant, C. (1997) *J. Electron Spectrosc. Relat. Phenom. 86*, 175−183.
36. Van Belzen, R., Kotlyar, A. B., Moon, N., Dunham, W. R., and Albracht, S. P. J. (1997) *Biochemistry 36*, 886−893.
37. Colpas, G. J., Maroney, M. J., Bagyinka, C., Kumar, M., Willis, W. S., Suib, S. L., Mascharak, P. K., and Baidya, N. (1991) *Inorg. Chem. 30*, 920−928.
38. Ressler, T. (1997) *J. Phys. IV 7*, C2−269.
39. Mustre de Leon, J., Rehr, J. J. Zabinsky, S. I., and Albers, R. C. (1991) *Phys. Rev. B44*, 4146−4156.
40. Rehr, J. J., and Albers, R. C. (1990) *Phys. Rev. B41*, 8139−8149.
41. Rehr, J. J., Zabinsky, S. I., and Albers, R. C. (1992) *Phys. Rev. Lett. 69*, 3397−3400.
42. Rosenfield, S. G., Armstrong, W. H., and Mascharak, P. M. (1986) *Inorg. Chem. 25*, 3014−3018.
43. Stewart, J. M., Lingafelter, E. C., and Breazeale, J. D. (1961) *Acta Crystallogr. 14*, 888−891.
44. Colpas, G. J., Day, R. O., and Maroney, M. J. (1992) *Inorg. Chem. 31*, 5053−5055.
45. Ghilardi, C. A., Sabatini, A., and Sacconi, L. (1976) *Inorg. Chem. 15*, 2763−2767.
46. Maroney, M. J., Colpas, G. J., Bagyinka, C., Baidya, N., and Mascharak, P. K. (1991) *J. Am. Chem. Soc. 113*, 3962−3972.
47. Maroney, M. J., Pressler, M. A., Mirza, S. A., Whitehead, J. P., Gurbiel, R. J., and Hoffman, B. M. (1995) *Adv. Chem. Ser. 246*, 21−60.
48. Kirby, J. A., Goodin, D. B., Wydrzynski, T., Robertson, A. S., and Klein, M. P. (1981) *J. Am. Chem. Soc. 103*, 5537−5542.
49. Müller, A., Erkens, A., Schneider, K., Müller, A., Nolting, H.-F., Sole, V. A., and Henkel, G. (1997) *Angew. Chem., Int. Ed. Engl. 36*, 1747−1750.
50. Roberts, L. M., and Lindahl, P. A. (1994) *Biochemistry 33*, 14339−14350.

51. Xia, J., Dong, J., Wang, S., Scott, R. A., and Lindahl, P. A. (1995) *J. Am. Chem. Soc. 117*, 7065−7070.
52. Nag, K., and Chakravorty, A. (1980) *Coord. Chem. Rev. 33*, 87−147.
53. Haines, R. I., and McAuley, A. (1981) *Coord. Chem. Rev. 39*, 77−119.
54. Lappin, A. G., and McAuley, A. (1988) *Adv. Inorg. Chem. 32*, 241−294.
55. Scarrow, R. C., Maroney, M. J., Palmer, S. M., Que, L., Jr., Roe, A. L., Salowe, S. P., and Stubbe, J. (1987) *J. Am. Chem. Soc. 109*, 7857−7864.
56. Garcin, E., Vernede, X., Hatchikian, E. C., Volbeda, A., Frey, M., and Fontecilla-Camps, J. C. (1999) *Structure 7*, 557−566.
57. Pierpont, C. G., and Eisenberg, R. (1972) *Inorg. Chem. 11*, 828−832.
58. Curtis, M. D., and Williams, P. D. (1983) *Inorg. Chem. 22*, 2661−2662.
59. Elbaze, G., Dahan, F., Dartiguenave, M., and Dartiguenave, Y. (1984) *Inorg. Chim. Acta 85*, L3−L5.
60. Miedaner, A., Curtis, C. J., Wander, S. A., Goodson, P. A., and DuBois, D. L. (1996) *Organometallics 15*, 5185−5190.
61. Fan, C., Teixeira, M., Moura, J., Moura, I., Huynh, B. H., Le Gall, J., Peck, H. D., Jr., and Hoffman, B. M. (1991) *J. Am. Chem. Soc. 113*, 20−24.

BI000300T